



Fermi National Accelerator Laboratory

FERMILAB-Pub-98/038-A

Quasar Photometry with the SDSS Monitor Telescope

Gordon T. Richards et al.

*Fermi National Accelerator Laboratory
P.O. Box 500, Batavia, Illinois 60510*

February 1998

Submitted to *Astronomical Society of the Pacific*

Operated by Universities Research Association Inc. under Contract No. DE-AC02-76CH03000 with the United States Department of Energy

Disclaimer

This report was prepared as an account of work sponsored by an agency of the United States Government. Neither the United States Government nor any agency thereof, nor any of their employees, makes any warranty, expressed or implied, or assumes any legal liability or responsibility for the accuracy, completeness, or usefulness of any information, apparatus, product, or process disclosed, or represents that its use would not infringe privately owned rights. Reference herein to any specific commercial product, process, or service by trade name, trademark, manufacturer, or otherwise, does not necessarily constitute or imply its endorsement, recommendation, or favoring by the United States Government or any agency thereof. The views and opinions of authors expressed herein do not necessarily state or reflect those of the United States Government or any agency thereof.

Distribution

Approved for public release; further dissemination unlimited.

Quasar Photometry with the SDSS Monitor Telescope

Gordon T. Richards

Department of Astronomy and Astrophysics, University of Chicago

richards@oddjjob.uchicago.edu

Brian Yanny, James Annis, and Heidi J. M. Newberg

Fermi National Accelerator Laboratory

yanny@sdss.fnal.gov, annis@sdss.fnal.gov, heidi@sdss.fnal.gov

Timothy A. McKay

Department of Physics, University of Michigan

mckay@umalp1.physics.lsa.umich.edu

Donald G. York

Department of Astronomy and Astrophysics, University of Chicago

don@oddjjob.uchicago.edu

and

Xiaohui Fan

Princeton University Observatory

fan@astro.princeton.edu

ABSTRACT

Photometric data were obtained for a set of known QSOs in five bands with a filter system similar to the Sloan Digital Sky Survey (SDSS) filter system for the purpose of testing the ability of the SDSS system to separate QSO colors from the colors of the stellar locus. Data were obtained from two similar telescopes and camera systems, and were intercompared. The F stars BD+26 2606 and BD+17 4708 were used as primary standards to set the zero points for the rest of the observed objects. The standard star magnitudes were found to be in reasonable agreement with the theoretically predicted magnitudes, and the QSO colors were well separated from the stellar locus, defined by random stars in the QSO fields.

1. The Sloan Digital Sky Survey Filters

The Sloan Digital Sky Survey (hereafter the Survey, or SDSS) has developed a new set of photometric filters, essentially broader versions of the Gunn-Thuan filters (Thuan and Gunn 1976), and named u' , g' , r' , i' and z' . The definitive absolute calibration of this filter system is in progress; the plan for calibration and approximate transformations are described in Fukugita et al (1996). Figure 1 shows the transmission curves for the SDSS filter set that was used for these observations. It should be pointed out that the various optical and detector elements that will be used for the actual survey will change slightly. Therefore we have designated the filter system used in our observations as u^* , g^* , r^* , i^* , and z^* . Any comparison of this data to future data will necessitate the use of a transformation between u^* and u' , etc. This paper does not attempt a definitive definition of the SDSS filter system, but rather gives a first set of measurements of objects in this system to verify their usefulness in using colors to separate stars from QSOs.

One goal of the Survey is to obtain spectra for approximately 100,000 quasi-stellar objects (QSOs). It is too time-consuming to take spectra of every stellar object in a field to look for QSOs. Multi-color photometry can be used to narrow down the search to a reasonable number of objects. Stars in general, but especially stars with strong lines of neutral hydrogen, are affected by the Balmer jump at 3648 Å. QSOs however, follow a power law spectrum and are not affected by the Balmer jump. As a result they have a higher u^* intensity relative to their intensity in g^* , which is red-ward of the Balmer jump, as compared to stars. Thus QSOs are generally more blue than stars, which can be seen readily by plotting $u^* - g^*$ vs. $g^* - r^*$. While it is difficult to say with certainty if a stellar-like image is a QSO from photometry, one can definitely determine which are likely candidates to be QSOs.

This program was begun as an experiment to test some of the facets of the Survey.

These include the ability to determine photometric conditions, the ability of the Monitor Telescope (MT) to be run in an automated or semi-automated fashion, and the ability of the SDSS filter system to distinguish between QSOs and the stellar locus. One of the purposes of taking the QSO data was to create a set of five color data, since no set currently existed, for the purpose of helping define target selection criteria. In addition, this work aided in the determination of the feasibility of conducting photometry at the 1 percent level at Apache Point Observatory, the site of the Survey, with the SDSS equipment. We set out to get data on 100 objects, and were able to get enough data to have an important impact on the planning of the SDSS.

2. The Observations

Table 1 provides a detailed description of the MT system, both as it was when this data was taken, and as it will be when the Survey begins. This is also compared to the telescope and instrument setup on the 1.0m at the U.S. Naval Observatory (USNO), a second site with a filter system identical to the one used on the MT. Table 2 indicates when and where the data was taken. A (P) indicates that the night was photometric, while (NP) means that it was not photometric, and the data from this night was not used. The (MP)'s mean that it was mostly photometric; however, at the USNO there is no instrumentation such as APO's 10μ cloud camera (Hull et al, 1994) to provide a basis for a consistent determination of photometricity.

2.1. Monitor Telescope at APO

The first set of observations was made with the Monitor Telescope (MT) of the Sloan Digital Sky Survey at Apache Point Observatory, Sunspot, New Mexico. The data

presented herein were taken during the period of July 22nd to July 26th 1995 during a period of excellent photometric conditions. Data were taken in only one filter each night in the order r^* , g^* , u^* , i^* , and z^* . In fact data were taken for a period of nearly 60 days during the summer. Most of it was useful for engineering and test purposes only. However, on these five nights, the telescope was operating reasonably well and more importantly the 10μ IR cloud camera and satellite maps showed no evidence of even a thin layer of cloud cover. While the zero point calibration of the cloud camera detector appears not to be stable, it was apparent that on these nights the cloud camera images were considerably cleaner than they had been on other relatively photometric nights. At most, atmospheric transparency varied by only a few percent, and was much less than other errors.

The QSO targets were a set of 31 bright QSOs ($V < 17$) selected from Hewitt and Burbidge (1993). The targets were selected from a list of QSOs with $V < 19$ that were chosen to be representative of a wide variety of QSOs, and QSO-like objects found in current catalogs. Interspersed between the QSOs were observations of Survey photometric standard stars, including some Landolt (1992) objects. Not all objects were observed in all bands.

The 0.6m Monitor Telescope is an $f/10$ Ritchey-Chrétien with an effective aperture area of 2210 cm^2 . The MT has a plate scale of approximately 33.333 arcseconds per millimeter. The CCD used for these observations was a SITE 512x512 detector with 27 micron pixels. Thus each pixel observes approximately 0.9 arcseconds of the sky and the whole chip sees about $8' \times 8'$ of the sky. A photon transfer curve was created using a series of pairs of dark and flat-field frames. The read noise for the CCD was measured to be approximately 15 electrons per pixel. See Table 1 for a full account of the telescope/CCD system.

Standard stars were observed in u^* , g^* , r^* , i^* , and z^* for 30,10,10,12, and 28 seconds

respectively. QSO exposure times were set according to the following formula,

$$\text{exptime} = 1.8 \times 10^{-5} * 10^{V/2.5}. \quad (1)$$

However, if this exposure time came out to be less than 30 seconds, then the exposure time was set to 30 seconds. This time was set so as to theoretically give a S/N of at least 100 in the u^* filter (unfortunately, not realized in all cases). The maximum exposure time in each filter was 214, 113, 71, 85, 200 seconds from blue to red, respectively. Plots of the standard star magnitudes were examined, and we find that errors of 0.2 mag, corresponding to a 5σ detection limit, were found at $u^*, z^* \sim 16$ mag, and $g^*, r^*, i^* \sim 17.25$ mag.

Only one filter was used each night, since the filter wheel box had not been installed prior to these observations. A flat-field frame was made for each night by taking the median of approximately 45 twilight flat images. Each twilight flat image was exposed so as to have the average pixel value to be nearly half of the full well value for the CCD. In addition, the average value of the bias of the images was used to do a bias subtraction on the images, and dark counts were assumed to be negligible.

The MT is designed to run in a completely automated fashion, and part of the purpose of these observations was to test this procedure. When the Survey begins, the MT will continuously observe standard stars and calibration patches on the sky from a list for the whole night with little or no input from the operator. The standard stars will be used to photometrically calibrate the patches which overlap areas of sky observed by the main survey 2.5-m telescope camera. These overlap areas then will be used to provide absolute photometric calibration for all objects in the survey good to a few percent, or better.

The automated routine first centers the telescope optical axis on an FK5 star near the program object, then the telescope moves to the program object and an exposure is made. Then the routine selects a standard star located in the vicinity of the QSO, and repeats the above sequence, using an appropriate exposure time in each case. Frequent focus corrections

were made by hand, as full automation of the telescope was not yet completed when the observations were made. FK5 stars were used merely to update positioning.

2.2. 1-m at USNO

The second set of observations were made with the 1.0-m telescope at the U.S. Naval Observatory (USNO) in Flagstaff, AZ, with a separate set of SDSS filters. This telescope was the first to use the Ritchey-Chrétien optical design and has an $f/7.2$ focal ratio, giving it a plate scale of $28''.125/\text{mm}$. The CCD used was a SITE 1024x1024 chip with 24μ pixels. Each pixel has size $0.''675$, and the field of view is approximately $11' \times 11'$. See Table 1 for complete system parameters.

Objects were observed in u^* for the first night with 10 to 60 second exposure times for standards and 1 to 5 min exposures for QSOs. On the second night g^* and r^* were observed with standard star exposure times from 2 to 4 seconds, and QSO exposure times from 12s to 4 min. In all, 38 QSOs were targeted, but not all were detected in all bands. No observations were made in i^* , or z^* . The 5σ detection limits (as described above for the MT) are $u^*, r^* \sim 18$, and $g^* \sim 19$.

The USNO data were flat-fielded and debiased as described above for the MT. Again the dark count was assumed to be negligible.

3. Data Reduction

Both data sets were reduced at Fermilab using SHIVA (Stoughton, 1995), the SDSS data processing software package, which is based on the TCL scripting language (Ousterhout 1994). After the images were debiased and flat-fielded as described above, a peak-finding algorithm picked out all of the objects on a frame and determined the number of counts

in a 4.5" and 3.3" radius for the MT and USNO telescopes respectively. An average (over the whole frame) sky value per pixel was also calculated for each frame and the number of pixels multiplied by this value was subtracted from the number of counts in an object.

Each corrected frame was then looked at to determine which object in the frame was the object of interest (either a standard star or QSO). The magnitude of all other objects was recorded and objects on different frames (in different filters) were matched up with a slightly different code, utilizing the same algorithm to determine the magnitudes. These field objects define the stellar locus and serve as comparison to the QSO data (galaxy contamination was minor at these magnitude levels). The results are discussed in the next section.

The code used to reduce the data was the same for both the data sets from both telescopes except for the fact that the CCD's are of different sizes, with different pixel scales (see Table 1). However, the data were reduced independently, and the data sets were later checked against one another.

In each filter, observations of one of the stars, BD+26 2606 or BD+17 4708, the defining F sub-dwarf standards in the Gunn-Thuan filter system (Oke and Gunn 1987), which are also the basis for the SDSS filter system, were used to determine the absolute zero point of each filter for each night. The zero point was defined such that instrumental magnitude plus the zero point was equal to the magnitude of BD+26 2606 or BD+17 4708 in a given filter as given in Table 3, taken from Fukugita et al. (1996), Table 7. Then, given these zero points for the MT, magnitudes were calculated for the rest of the objects using the following formulas,

$$u^* = -u_o^* + 18.17 - 0.6 * (AM - 1.088) \quad (2)$$

$$g^* = -g_o^* + 20.29 - 0.25 * (AM - 1.086) \quad (3)$$

$$r^* = -r_o^* + 20.20 - 0.1 * (AM - 1.080) \quad (4)$$

$$i^* = -i_o^* + 19.81 - 0.08 * (AM - 1.080) \quad (5)$$

$$z^* = -z_o^* + 18.71 - 0.06 * (AM - 1.097), \quad (6)$$

where AM is the airmass, and the first term (u_o^* , etc.) is the measured instrumental magnitude (log of the count rate multiplied by 2.5). Note that the third term gives a rough correction for atmospheric extinction and the term subtracted from the air mass of the observation is the average air mass at which the objects used to calculate the zero points were taken. The coefficients of extinction are not directly based upon measurement. These values were determined by taking the values of extinction for the Gunn-Thuan filters at the Palomar 1.5-m, as given by Kent (1985), and transforming to the SDSS filter set. Use of these values is acceptable since the largest extinction corrections are expected to be less than 0.07 mag, thus errors in the correction to the correction will be negligible for our present purposes. These coefficients will be determined from observations in the Survey. The second term is the zero point as determined from the primary standards. Similar equations were derived for the USNO data.

The results of the data reduction are presented in the following section. In addition an extensive review of the errors is given following the presentation of results.

4. Results

After reducing each data frame, the multiple observations for a given object at each telescope were combined.

Early QSO surveys, e.g. Green, Schmidt, and Liebert (1986), found many QSOs with UV excesses at $z < 2$, from photographic surveys with UBV filters. More recent efforts by Warren et al. (1991) and Kron et al. (1991) utilized longer wavelength filters to find QSOs at higher redshifts. As the Lyman α line moves into redder bands, QSOs with

$z > 3.1, 3.7,$ and 4.7 can be distinguished from the stellar locus with $u^*g^*r^*, g^*r^*i^*,$ and $r^*i^*z^*$ color-color plots, respectively, because of the structure associated with QSOs by Lyman- α emission and intergalactic H I absorption. (Schneider, Schmidt and Gunn 1991)

Tables 4 and 5 show the results of the QSO measurements for the MT and USNO data respectively. Again both sets agree well for the few objects which have data taken in both systems.

Figures 2 and 3 display the $u^* - g^*$ vs. $g^* - r^*$ color-color diagrams for the MT and USNO data respectively, plotting the QSOs (small numbers), standard stars (boxes), and the stellar locus (dots). The QSOs are plotted with small numbers indicating $10 \times$ redshift to give one an idea of how redshift affects QSO colors.

The two stellar loci from the MT and USNO data are coincident within the errors, indicating that the filter systems are equivalent. Since the stars making up the stellar loci were random objects which happened to lie in the field of the QSOs, they are representative of late-type stars in the Galactic disk, with negligible contributions from early-type stars, spheroidal population objects, and extra-galactic sources. In the region of color space significantly more blue than the blue end of the stellar locus, where we expect to see blue stars, only 10 to 30 percent of the objects were not QSOs, for the MT and USNO respectively. In addition, about 75 percent of the QSOs examined were well outside the stellar locus in the $u^* - g^*, g^* - r^*$ color-color diagram. The total area sampled is estimated to be 2 square degrees. There were approximately 150 and 650 objects detected in all three (u^*, g^*, r^*) bands for the MT and USNO respectively. The observed stellar loci agree well with the theoretical locus. Theoretical magnitudes were calculated for all of our standard stars by taking the V magnitude and B-V color and converting to SDSS magnitudes (Kent 1996, private communication). The standard deviation of the difference between our observed magnitudes and the calculated magnitudes are given with the error measurements

in column 1 of Table 6. It should be noted that the large discrepancy in u^* is partially the result of differences in the filter response used compare to that used for the calculations. The values for i^* and z^* are not useful, since the transformation does not extrapolate to the red. More accurate theoretical calculations have been produced by taking stellar spectra from Gunn and Stryker (1983) and converting them to SDSS colors (Fukugita et al. 1996). A detailed comparison of theoretical to observed magnitudes is forthcoming (Lenz et al. 1996, in preparation).

We show the mean track of a Monte-Carlo simulation of quasar colors from the quasar spectra according to observed distribution of power law indices and emission line strength, Lyman alpha and Lyman Limit absorptions from $z=0.4$ to $z=6$ (Fan et al., 1996, in preparation). The colors that each simulated QSO spectrum produced in the SDSS filter system were calculated. These colors are plotted in Figures 2–6, with the QSO’s z plotted in large figures as $10\times$ redshift. The observed data shows a broad scatter in true QSO color, even for QSOs with similar redshifts. For example, QSOs in the redshift range $z = 1.7 - 1.9$ show a spread in $g^* - r^*$ color of 0.5 mag. QSOs with a $1.9 \leq z \leq 2.7$ show a spread of ~ 1 mag in $u^* - g^*$. This can be contrasted with the tightness of the stellar locus $\Delta(u^* - g^*) \leq 0.4$ mag, $\Delta(g^* - r^*) \leq 0.2$ mag. Thus, various QSO properties such as emission line flux, continuum slope, intrinsic reddening, and amount of absorption along the line of sight contribute to the spread in color. It should be pointed out that the model curves actually represent typical values for intrinsic QSO properties, and that the model QSO color curves should really be a shaded bands, rather than curves; however, the true theoretical QSO locus is consistent with the observed spread. We have plotted the curves by taking approximately the mean values of the parameters for the model QSO.

Figures 4, 5, and 6 are similar to the first except that now we plot $g^* - r^*$ versus $r^* - i^*$, and $r^* - i^*$ versus $i^* - z^*$ for both the MT and USNO data. There were 550 and 150 objects detected in the (g^*, r^*, i^*) bands for the MT and USNO respectively. The $i^* - z^*$ data in

Figure 6 is limited in usefulness for detection of low redshift ($z < 4.6$) QSOs; however, it is a good discriminant for higher redshift objects, as the indicated theoretical QSO locus shows. For this color 350 objects were detected. It should be noted that the QSO whose redshift is 3.6 in Figure 4 is the gravitational lens system, B 1422 + 231. It is thought that this point may be affected by the lensing object, and may not represent the true color of the QSO.

To demonstrate the random photometric errors as a function of magnitude for the data, Figure 7 shows a color-magnitude diagram with error bars for QSOs and standard stars in the MT data set.

5. Errors

The circumstances under which the MT observations were made dictate the need for an extensive discussion of errors. The observations presented herein were taken during a time when the MT was being run in a test state. That is, we were trying to take real data with the telescope for scientific purposes to expose engineering and other problems.

It was discovered that the equatorial mount telescope was not perfectly aligned with the North Celestial Pole, which made it difficult to track accurately for more than a few minutes. Coarse re-focusing was done every five sets of measurements, where a set consisted of 2 FK5 stars, a QSO, and a standard star. The camera had higher than anticipated noise characteristics, which resulted in lower than expected signal to noise. All of these problems either have been or will be corrected before the Survey proper begins.

We have calculated a random error term for each measurement for the MT (and for the USNO data as well). This error is given by

$$\text{error} = \frac{\sqrt{\text{obj.cnts} \times \text{gain} + \text{skycnts}/\text{pix} \times \text{gain} \times \text{no.pixels} + \text{rdnoise}^2 \times \text{no.pixels}}}{\text{obj.cnts} \times \text{gain}}, \quad (7)$$

using a gain of 9.39 and 7.43 electrons/ADU and a read noise of 15 and 6 electrons for the MT and USNO data, respectively. The object count is the sum over all the pixels in the apertures defined earlier and the number of pixels refers to the number of pixels in the aperture.

In addition to this random error for each object, a standard deviation was calculated for each night for the MT data, representing the data from one filter. This standard deviation was calculated from multiple observations of the standard star GCRV 9483. The magnitudes from these multiple observations were averaged together for each filter and the variance obtained. We also did this calculation for a few other stars of differing colors for each filter. These calculations are consistent with those for GCRV 9483, except we note that the standard deviation quoted for the r^* filter may be a bit high, as seen in column 2 of Table 6, but there are not enough observations of the other stars to say for sure.

As noted, the extinction coefficients are not well determined from our present small data set, and we have thus simply applied a general correction based on theoretical calculations extrapolated from older photometric systems.

We have attempted to get an idea of the systematic errors on the zero points by comparing the data taken with the MT to data taken at the USNO, for the six standard stars the are in both data sets. We have calculated an average difference between the two data sets for the u^* , g^* , and r^* filters, and the results are shown in column 3 of Table 6.

We should also point out that we have made no attempt to correct for color term differences between the two telescope/filter systems. The u^* filter will be changing as stated above and the chip will be replaced with a slightly different one, so one must consider that

these data represent the older system. However, it is encouraging that the systematic errors between the MT and USNO data do not depend significantly on the colors of the standards, indicating that the colors terms will be small. Ten of the QSOs were observed with both telescopes. Most of the measurements agree within the 1σ photometric errors in magnitude, and all of the measurements agree within 3σ . This means that QSO selection for the Survey should not be adversely affected by variability of QSOs or quasars on the timescale of a few months. However, we should point out that a few of our images were well underexposed as a result of setting exposure times based on published magnitudes.

The total error on each measurement is somewhat complicated to derive. The true error for each measurement should take into account the random error for a given object, the standard deviation, and the systematic error for that night; however, Figure 7 depicts only the photon noise error.

6. Conclusions

We have shown that the SDSS filter system does a good job of separating the QSOs from the stellar locus. The SDSS magnitudes for a set of well known standard stars and QSOs serve as an initial data set until the filter system is formally calibrated. We caution that corrections of order 0.1 mag will be present in some of these numbers when compared with the final SDSS filter calibration. The photon noise errors in the USNO data set are smaller than those in the MT data. The filters, in particular the u^* and g^* filters, enable us to do an excellent job of picking out QSO candidate based on color, for objects with $z < 2.5$. QSOs with $z > 3.1$ can be distinguished using one or more of the color-color plots.

We are grateful to Jeff Pier and the USNO for use of their 1-m telescope and their SDSS filter system. We thank Donald Schneider for his help with interpreting theoretical

QSO tracks, and Dawn Lenz for deriving theoretical stellar loci in the SDSS filter system. We acknowledge support from Ron Rechenmacher, Tom Nicinski and Don Petravick of Fermilab in assembling the Monitor telescope CCD system. We thank Fritz Bartlett for reading an early draft of the manuscript. We also thank an anonymous referee for constructive comments regarding theoretical QSO colors. GTR was supported in part by an Adler Fellowship.

Table 1
Telescope and Camera Systems

Component	MT (as used)	MT (as planned)	USNO 1-m
Camera and CCD:			
Maker	SITe	SITe	SITe
Size	512x512	2048x2048	1024x1024
Type	Thinned	Thinned	Thinned
Coating	UV/AR	UV/AR	UV/AR
Illumination	back	back	back
Pixel size	27 μ	24 μ	24 μ
Pixel scale	0.9"/pix	0.82"/pix	0.675"/pix
Read noise	15 e ⁻	10 e ⁻	6 e ⁻
Gain	9.39 e ⁻ /ADU	4.5 e ⁻ /ADU	7.43 e ⁻ /ADU
Full well	300,000 e ⁻	300,000 e ⁻	300,000 e ⁻
Serial No.	1615HR33-05	4271ABU12	4292BCU-09-04
Telescope:			
Size	0.6m	0.6m	1.0m
Type	Ritchey-Chrétien	Ritchey-Chrétien	Ritchey-Chrétien
f ratio	f/10	f/10	f/7.2
Corrector	No	Gascoigne corrector and field flattener	Yes
Plate scale	33.333"/mm	34.167"/mm	28.125"/mm
Field Size	7.7' × 7.7'	28.0' × 28.0'	11.5' × 11.5'
Mirror coatings	MgF	MgF	MgF

Table 1:

Table 2
Days of Observation

Filter	MT Date Observed	USNO Date Observed
u*	24 July (P)	21 Nov. (NP), 22 Nov. (MP)
g*	23 July (P)	23 Nov. (MP)
r*	22 July (P)	24 Nov. (MP)
i*	25 July (P)	25 Nov. (NP), 26 Nov. (NP)
z*	26 July (P)	25 Nov. (NP), 26 Nov. (NP)

Table 2:

Table 3
Primary Standard Magnitudes

Filter	BD+26 2606	BD+17 4708
u*	10.79	10.57
g*	9.90	9.64
r*	9.61	9.35
i*	9.52	9.25
z*	9.50	9.23

Table 3:

Table 4
MT QSO Magnitudes

Object	redshift	u^*	g^*	r^*	i^*	z^*
PG 1718+481	1.08	15.03 ± 0.17	14.78 ± 0.03	14.50 ± 0.02	14.46 ± 0.03	14.28 ± 0.06
MARK 876	0.13	15.00 ± 0.09	15.09 ± 0.04	14.91 ± 0.03	14.44 ± 0.03	14.46 ± 0.04
PG 0026+12	0.14	15.44 ± 0.14	15.25 ± 0.04		14.62 ± 0.04	14.62 ± 0.04
PG 0052+251	0.15	15.36 ± 0.12	15.31 ± 0.04		14.78 ± 0.04	14.94 ± 0.06
PG 1700+518	0.29	15.61 ± 0.15	15.39 ± 0.05	14.99 ± 0.04	14.83 ± 0.04	14.46 ± 0.04
IRAS 21219-1757	0.11	15.88 ± 0.59	15.39 ± 0.06	15.36 ± 0.05	14.98 ± 0.05	14.79 ± 0.12
Q 1435-0134	1.31		15.55 ± 0.04	15.36 ± 0.03	15.33 ± 0.04	15.48 ± 0.06
MARK 813	0.13		15.67 ± 0.06	15.58 ± 0.06	15.10 ± 0.06	
MARK 877	0.11	15.59 ± 0.15	15.70 ± 0.06	15.74 ± 0.07	15.24 ± 0.06	15.23 ± 0.08
4C 09.72	0.43	15.97 ± 0.14	15.73 ± 0.04	15.83 ± 0.05	15.73 ± 0.06	15.44 ± 0.05
PG 1538+477	0.77	16.14 ± 0.14	15.75 ± 0.04	15.72 ± 0.04	15.78 ± 0.06	15.51 ± 0.06
3C 351.0	0.37	16.04 ± 0.27	15.76 ± 0.07	15.45 ± 0.05	15.42 ± 0.07	14.93 ± 0.06
PKS 2349-01	0.17	15.77 ± 0.23	15.86 ± 0.08	15.69 ± 0.07	15.30 ± 0.07	15.22 ± 0.08
PG 1715+535	1.93	16.53 ± 0.13	15.89 ± 0.03	15.47 ± 0.02	15.25 ± 0.02	15.24 ± 0.03
PG 2302+029	1.05	16.13 ± 0.20	15.89 ± 0.06	15.71 ± 0.06	15.74 ± 0.07	15.49 ± 0.07
TON 256	0.13	15.93 ± 0.20	15.91 ± 0.07	15.65 ± 0.06	15.17 ± 0.06	15.27 ± 0.08
PKS 0044+030	0.62		15.92 ± 0.03		15.94 ± 0.02	15.78 ± 0.03
PG 1630+377	1.48	16.27 ± 0.15	16.13 ± 0.06	15.94 ± 0.05	15.83 ± 0.06	15.70 ± 0.07
PKS 2340-036	0.90	16.41 ± 0.22	16.14 ± 0.07	16.02 ± 0.06	16.01 ± 0.07	15.93 ± 0.08
PKS 2344+09	0.67	16.20 ± 0.17	16.15 ± 0.07	16.02 ± 0.07	15.88 ± 0.07	15.81 ± 0.08
HS 1700+6416	2.72	16.90 ± 0.27	16.19 ± 0.06	16.04 ± 0.06	15.96 ± 0.06	15.94 ± 0.08
UM 18	1.90	16.39 ± 0.16	16.32 ± 0.06		15.94 ± 0.06	15.73 ± 0.06
B 1422+231	3.62		16.33 ± 0.05	15.18 ± 0.02	15.07 ± 0.02	
Q 1442+295	2.67	17.34 ± 0.36	16.46 ± 0.07	16.32 ± 0.07	16.23 ± 0.07	
SBS 1425+606	3.20		16.50 ± 0.06	16.34 ± 0.05	16.26 ± 0.06	
S4 1435+63	2.06		16.55 ± 0.09	16.50 ± 0.09	16.34 ± 0.09	15.66 ± 0.06
KUV 16313+3931	1.02	17.16 ± 0.35	17.03 ± 0.14	16.73 ± 0.12	16.73 ± 0.14	
KP 1623.7+26.8B	2.52	17.68 ± 0.57	17.28 ± 0.17	17.26 ± 0.19	17.25 ± 0.23	
PKS 2126-15	3.27		17.37 ± 0.09	16.96 ± 0.06	16.78 ± 0.06	16.34 ± 0.06
3C 345.0	0.59		17.74 ± 0.28	17.61 ± 0.27	17.39 ± 0.27	
PG 1634+706	1.33	14.92 ± 0.15		14.41 ± 0.02	14.35 ± 0.03	14.22 ± 0.05

Table 4:

Table 5
USNO QSO Magnitudes

Object	redshift	u^*	g^*	r^*
PG 0804+761	0.10	14.31 ± 0.01	14.75 ± 0.01	14.93 ± 0.01
PKS 0405-12	0.57	15.29 ± 0.02	14.83 ± 0.01	14.74 ± 0.01
PG 0026+12	0.14	15.39 ± 0.02	15.24 ± 0.01	14.96 ± 0.01
PG 0052+251	0.15	15.31 ± 0.02	15.28 ± 0.01	15.15 ± 0.01
PG 0844+349	0.06	15.18 ± 0.03	15.28 ± 0.01	14.96 ± 0.01
NAB 0205+02	0.15	15.60 ± 0.02	15.31 ± 0.01	15.21 ± 0.01
PG 0953+415	0.24		15.45 ± 0.01	15.43 ± 0.01
4C 09.72	0.43	16.00 ± 0.03	15.72 ± 0.02	15.74 ± 0.03
PG 2302+029	1.05	16.12 ± 0.07	15.76 ± 0.02	15.55 ± 0.03
PG 0117+213	1.49	16.23 ± 0.03	15.95 ± 0.01	15.67 ± 0.01
PKS 0044+030	0.62	16.25 ± 0.04	16.07 ± 0.02	15.95 ± 0.03
PKS 2349-01	0.17	16.01 ± 0.03	16.07 ± 0.03	15.90 ± 0.02
PKS 2340-036	0.90	16.47 ± 0.04	16.11 ± 0.02	15.93 ± 0.03
PKS 2344+09	0.67	16.73 ± 0.06	16.13 ± 0.02	15.99 ± 0.02
3C 232	0.53		16.16 ± 0.01	16.02 ± 0.01
MARK 132	1.75		16.17 ± 0.01	16.01 ± 0.01
3C 110	0.77	16.69 ± 0.04	16.25 ± 0.01	16.13 ± 0.01
PG 0935+416	1.94	16.43 ± 0.02	16.28 ± 0.01	16.24 ± 0.01
UM 18	1.90	16.40 ± 0.03	16.32 ± 0.01	16.13 ± 0.01
UM 673	2.72	17.35 ± 0.07	16.63 ± 0.01	16.47 ± 0.01
PHL 957	2.68	17.50 ± 0.08	16.64 ± 0.01	16.36 ± 0.01
MS 03180-1937	0.10		16.90 ± 0.02	16.34 ± 0.03
S5 0836+71	2.17	17.00 ± 0.03	17.02 ± 0.01	14.67 ± 0.01
TB 0933+733	2.52	17.97 ± 0.03	17.12 ± 0.01	17.04 ± 0.01
Q 0018-0220	2.56		17.20 ± 0.01	16.95 ± 0.01
PKS 2126-15	3.27		17.40 ± 0.11	16.96 ± 0.14
SBS 0953+549	2.58		17.56 ± 0.01	17.43 ± 0.01
Q 0302-0000	3.29		17.69 ± 0.01	17.45 ± 0.01
0956+1217	3.30		17.86 ± 0.01	17.50 ± 0.01
Q 0256-0000	3.37		17.92 ± 0.01	17.59 ± 0.01
PKS 0215+015	1.72	19.43 ± 0.41	18.87 ± 0.16	18.31 ± 0.07
PKS 0219-164	0.70		18.99 ± 0.14	18.79 ± 0.06
0846+51W1	1.86		20.33 ± 0.14	
S4 0902+49	2.69	18.38 ± 0.03		
Q 2231-0015	3.02	19.36 ± 0.34		

Table 5:

Table 6

Errors

filter	theory vs. obs. ¹	std. dev. ²	sys. err. ³
u^*	0.374	0.020	0.06
g^*	0.091	0.007	0.05
r^*	0.033	0.025	0.10
i^*		0.013	
z^*		0.014	

¹ Std. dev. of theoretical mag. minus obs. mag.

² Std. dev. of obs., magnitudes

³ Diff. between MT and USNO magnitudes

Table 6:

REFERENCES

Fan, X.-H. et al., 1996, in preparation

Fukugita, M., Ichikawa, T., Gunn, J.E., Doi, M., Shimasaku, K., and Schneider, D.P., 1996,
AJ, 111, 1748

Gunn, J. E., & Stryker, M.M., 1983, ApJS, 52, 121

Green, R.F., Schmidt, M., and Liebert, J., 1986, ApJS, 61, 305

Hewitt, A., and Burbidge, G., 1993, ApJS, 87, 451

Hull, C.L., Limmongkol, S.L., and Siegmund, W.A., 1994, Proc. SPIE, 2199

Kent, S.M., 1985, PASP, 97, 165

Kent, S.M., 1996, private communication

Kron, R.G., Bershad, M.A., Munn, J.A., Smetanka, J.J., Majewski, S., and Koo, D.C.,
1991, ASP Conference Series, 21, 32

Landolt, A.U., 1992, AJ, 104, 340

Lenz, D. et al., 1996, in preparation

Oke, J.B., and Gunn, J.E., 1987, ApJ, 266, 713

Ousterhout, J. K., 1994, Tcl and the Tk Toolkit (Reading, Massachusetts: Addison-Wesley)

Schneider, D.P., Schmidt, M., and Gunn, J.E., 1991, AJ, 101, 2004

Stoughton, C., 1995, BAAS, 187, 9101

Thuan, T.X., and Gunn, J.E., 1976, PASP, 88, 543

Warren, S.J., Hewett, P.C., Irwin, M.J., and Osmer, P.S., 1991, ApJ, 76, 1

Figure Captions

Fig. 1.— Transmission curves for the MT filter set used in this paper. Transmission is plotted for airmasses of 0.0 (above the atmosphere) and 1.2.

(Gunn, private communication, 1996)

Fig. 2.— $u^* - g^*$ plotted versus $g^* - r^*$ for standard stars, field stars, QSOs, and the stellar locus. QSOs are indicated by $10 \times$ redshift (in small figures) to aid in the assessment of the effects of redshift on their colors. The solid line is a theoretical QSO, redshifted from $z = 0.4$ to $z = 5.5$, with large figures indicating $10 \times$ redshift.

Fig. 3.— Same as above, but with USNO data.

Fig. 4.— $g^* - r^*$ plotted versus $r^* - i^*$ for MT data.

Fig. 5.— Same as above, but with USNO data.

Fig. 6.— $r^* - i^*$ plotted versus $i^* - z^*$ for MT data.

Fig. 7.— $g^* - r^*$ vs. r^* color-magnitude diagram with error bars for MT standards and QSOs.

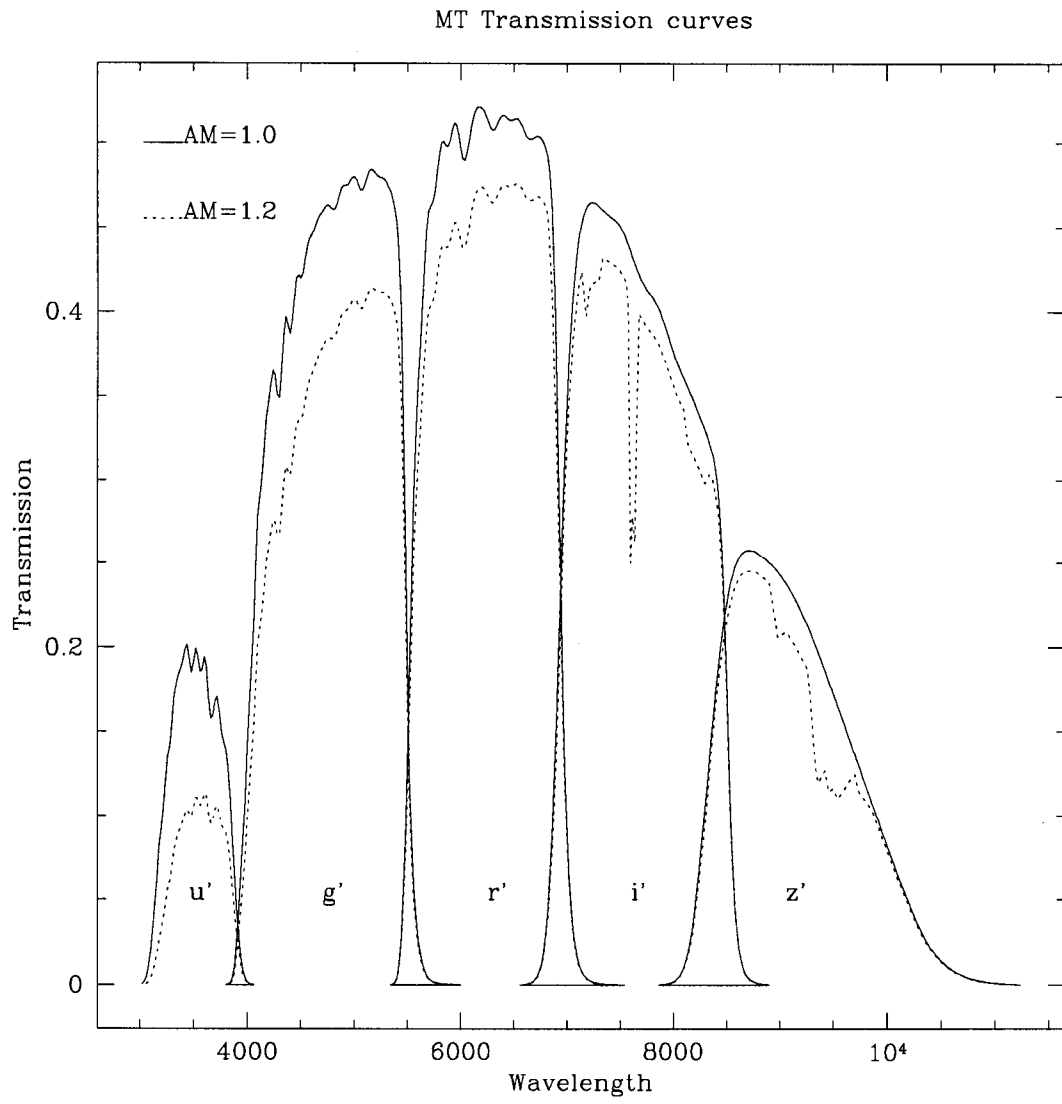


Fig. 1.—

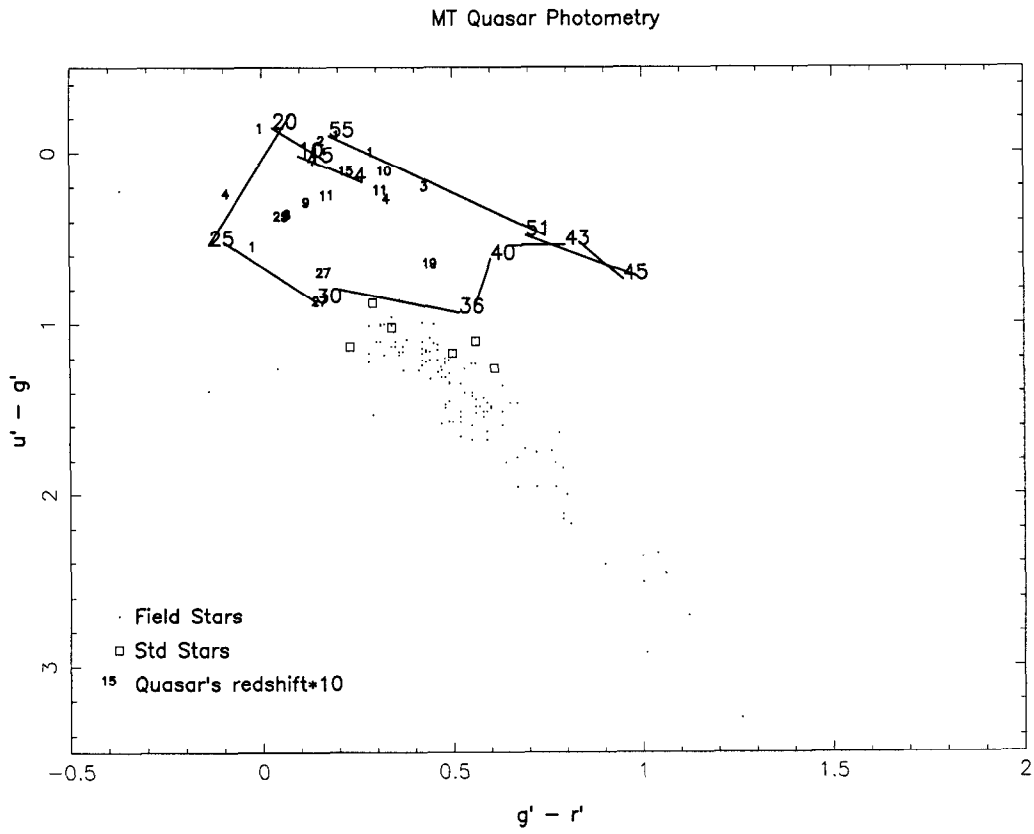


Fig. 2.—

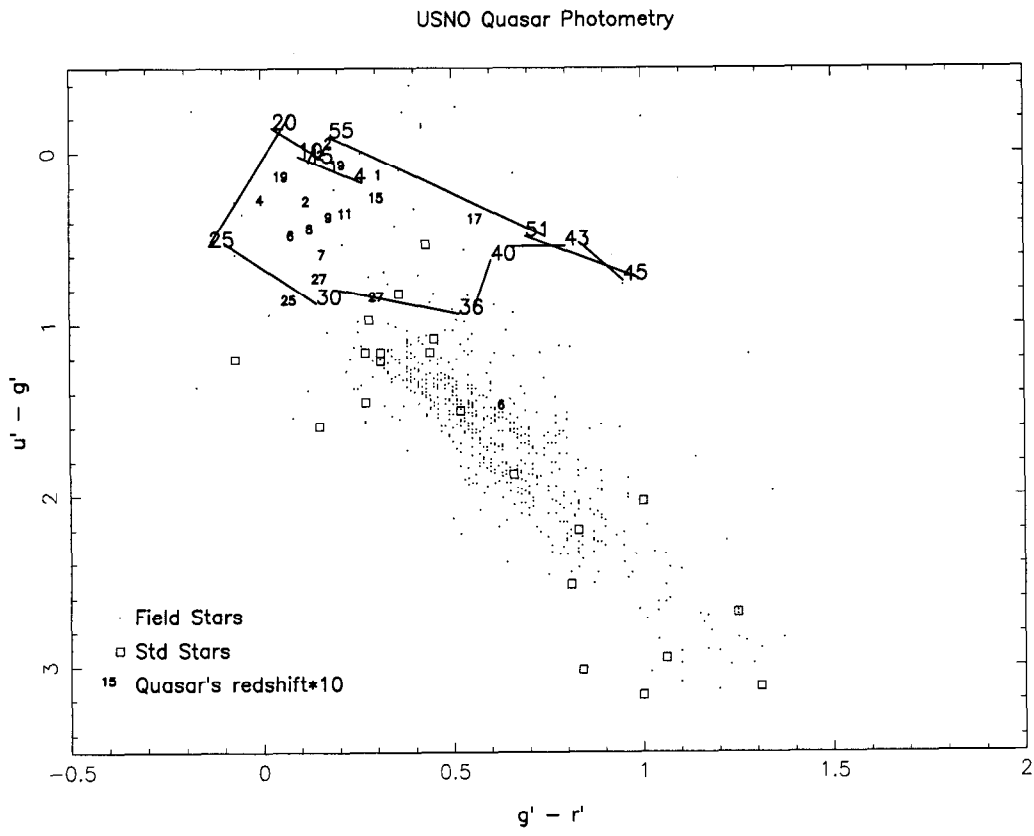


Fig. 3.—

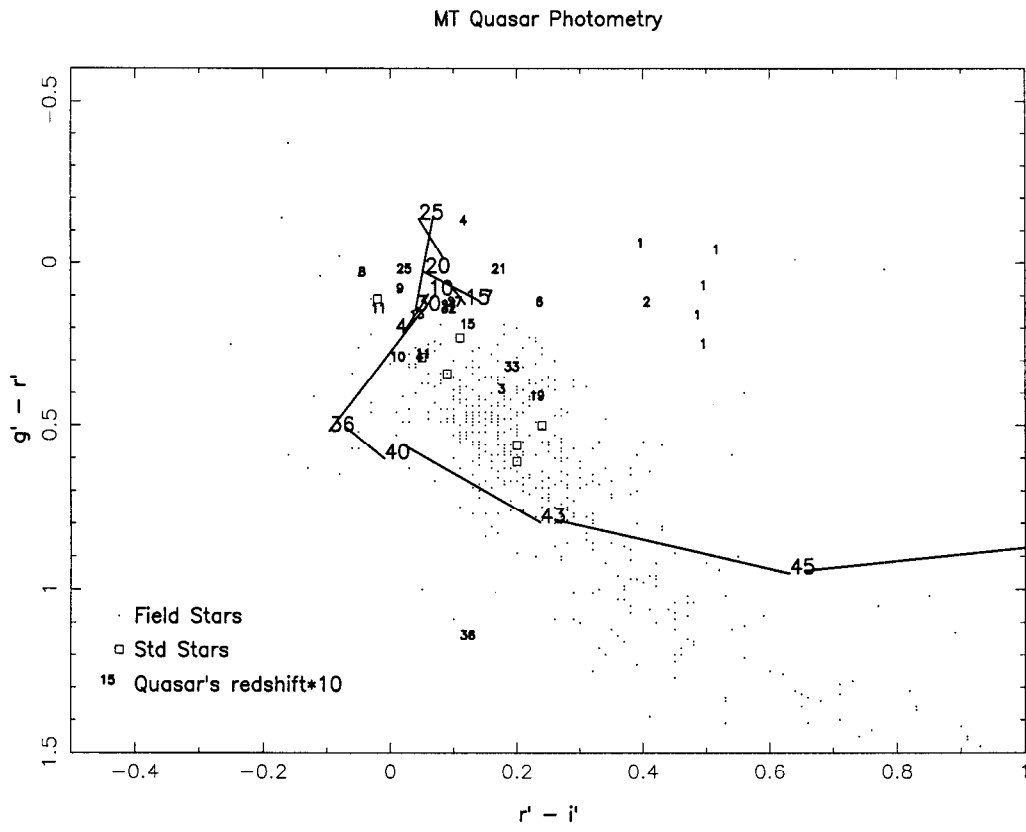


Fig. 4.—

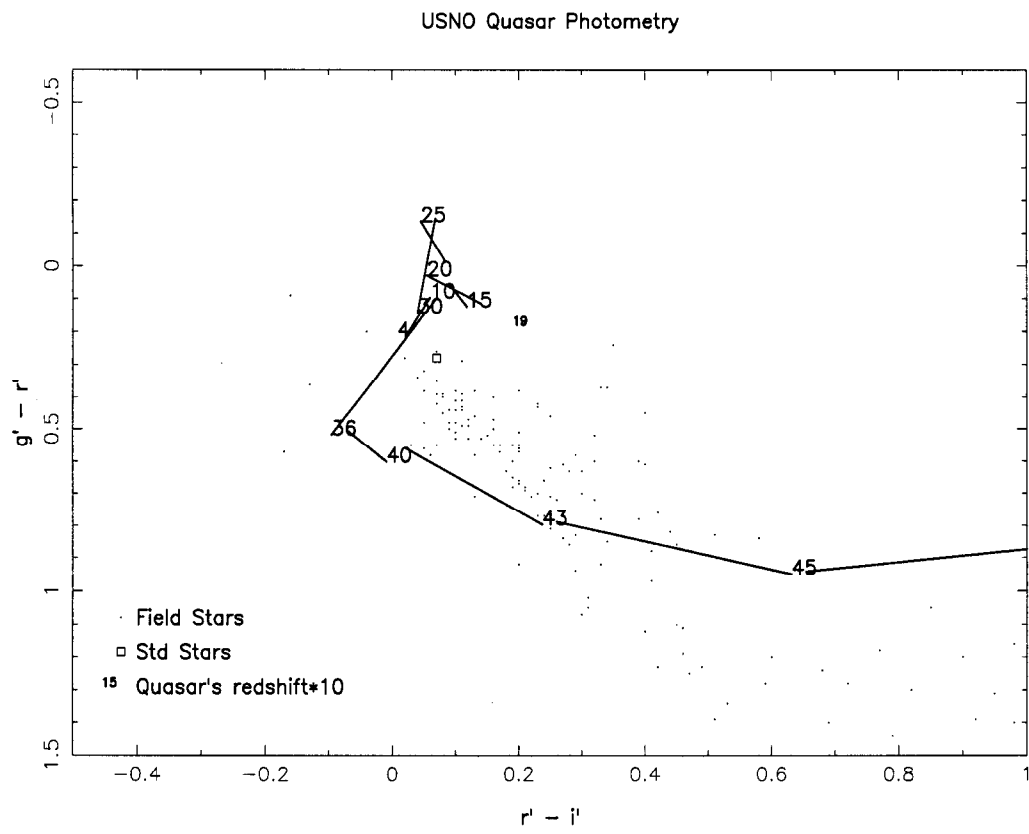


Fig. 5.—

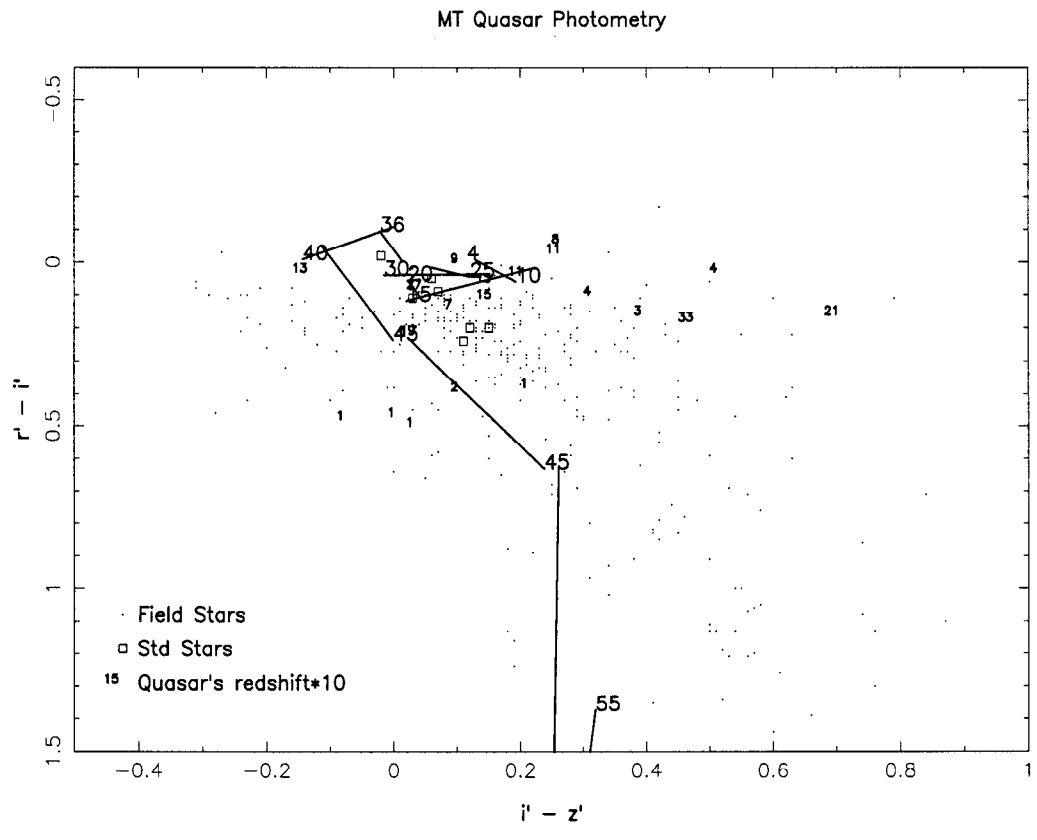


Fig. 6.—

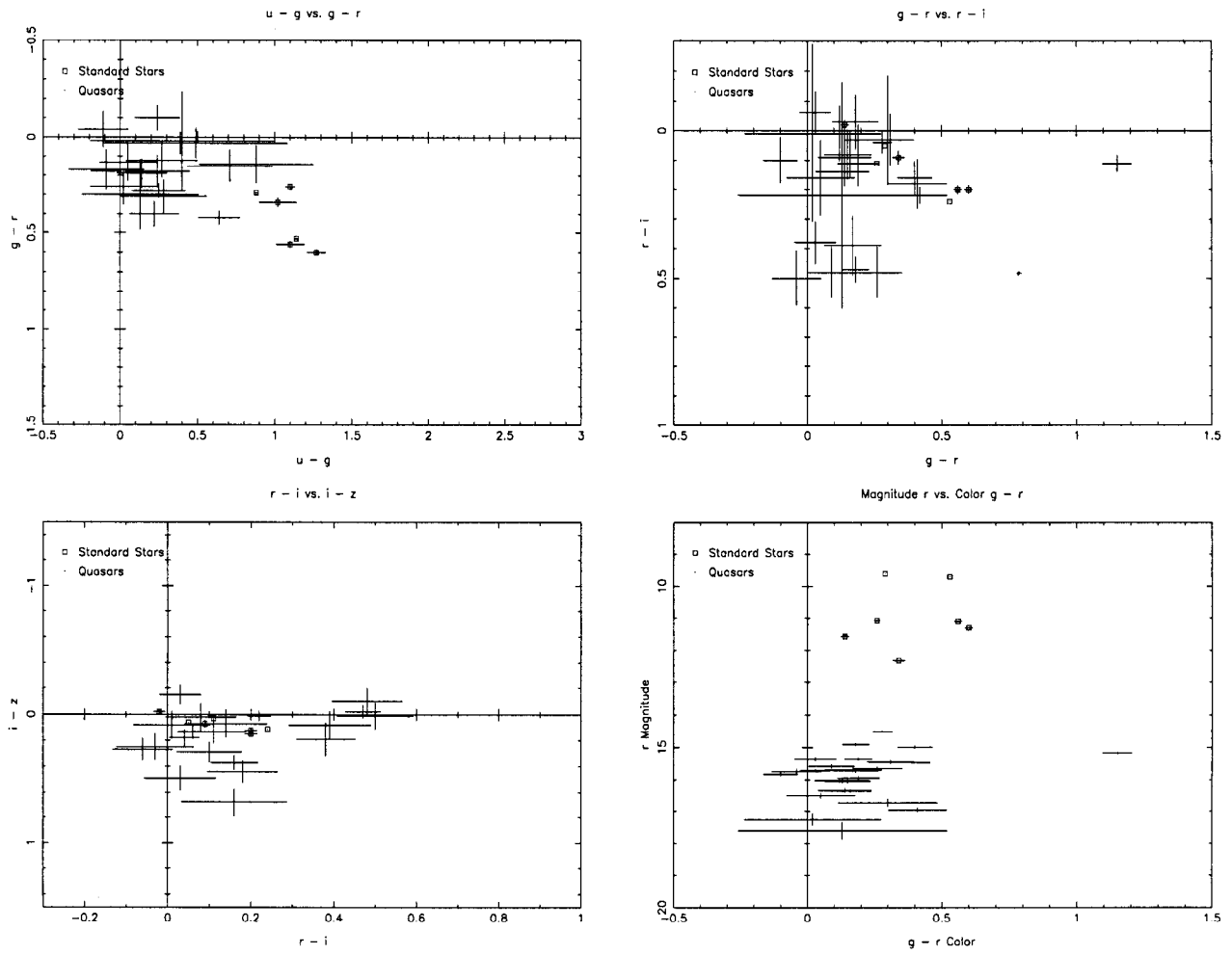


Fig. 7.—